

# Synthesis of 3D porous ceramic scaffolds obtained by the sol-gel method with surface morphology modified by hollow spheres for bone tissue engineering applications

E. Sebastián<sup>a</sup>, A. Murciano<sup>b</sup>, P.N. De Aza<sup>a</sup>, P. Velasquez<sup>a,\*</sup>

<sup>a</sup> Instituto de Bioingeniería, Universidad Miguel Hernández, Avda. Universidad s/n, Elche, Alicante, 03202, Spain

<sup>b</sup> Departamento de Materiales, Óptica y Tecnología Electrónica, Universidad Miguel Hernández, Avda. Universidad s/n, Elche, Alicante, 03202, Spain

## ARTICLE INFO

### Keywords:

Sol-gel processes  
Surfaces  
Biomedical applications  
Delivery systems

## ABSTRACT

In the present work, we modified the surface morphology of 3D porous ceramic scaffolds by incorporating strontium phosphate (SrP) hollow nano-/microspheres with potential application as delivery system for the local release of therapeutic substances. SrP hollow spheres were synthesized by a template-free hydrothermal method. The influence of the reaction temperature, time and concentration of reactants on precipitates' morphology and size were investigated. To obtain a larger number of open hollow spheres, a new methodology was developed consisting of applying a second hydrothermal treatment to spheres by heating them at 120 °C for 24 h. The X-ray diffraction (XRD) analysis indicated that spheres consisted of a main magnesium-substituted strontium phosphate phase ((Sr<sub>0.86</sub>Mg<sub>0.14</sub>)<sub>3</sub>(PO<sub>4</sub>)<sub>2</sub>). The scanning electron microscopy (SEM) micrographs confirmed that spheres had hollow interiors (~350 nm size) and an average diameter of 850 nm. Spheres had a specific surface area of 30.5 m<sup>2</sup>/g, a mesoporous shell with an average pore size of 3.8 nm, and a pore volume of 0.14 cm<sup>3</sup>/g. These characteristics make them promising candidates for drug, cell and protein delivery. For the attachment of spheres to scaffolds' surface, ceramic structures were immersed in an ethanol solution containing 0.1 g of hollow spheres and kept at 37 °C for 4 h. The scaffolds with incorporated spheres were bioactive after being immersed in simulated body fluid (SBF) for 7 days and spheres were still adhered to their surface after 14 days.

## 1. Introduction

In recent years, many studies have focused on developing local delivery systems for biomedical applications. Different structures like rods, fibers, tubes, needles and spheres have been studied as drug carriers [1, 2]. These structures have different loading and releasing efficiencies. Of them, hollow structures, especially hollow spheres on the nano-/microscale, have shown great potential as controlled delivery systems for biomedical applications thanks to their unique characteristics, such as high surface area, large pore volume, low density, and morphology with hollow interiors [3,4]. The hollow cavity confers them much higher loading capacity compared to other types of structures, allowing them to locally deliver a variety of compounds like proteins, cells, genes and especially drugs [5,6].

Several methods have been used to fabricate hollow spherical structures, including spray-drying, sol-gel, the template method, microemulsions, microwave synthesis and the hydrothermal method

[6–10]. The template method has been the most widely used technique to prepare hollow spheres. These templates can be either hard, mainly polymers, silica and carbon-based templates, or soft, emulsion droplets, vesicles, micelles, and gas bubbles [3,11]. Their main drawback is the need to remove the template once the synthesis process finishes. Template removal is not only a complicated time-consuming process, but it can also affect the morphology and structural integrity of the final products, limiting their practical applications. As an alternative, template-free strategies, such as the Ostwald ripening process in combination with the hydrothermal method have been studied [12,13]. This approach does not require any kind of templating, which simplifies the synthesis of hollow spheres and, is therefore, the method that was herein followed.

Considering the biocompatibility, biodegradability and toxicity of carriers, hollow spheres can be prepared from different materials like natural or synthetic polymers, such as collagen, chitosan, alginate and poly(lactic-co-glycolic acid) (PLGA), or ceramics like calcium

\* Corresponding author. Instituto de Bioingeniería, Universidad Miguel Hernández, Avda. Universidad s/n, Elche, Alicante, 03202, Spain.

E-mail address: [pavelasquez@umh.es](mailto:pavelasquez@umh.es) (P. Velasquez).

<https://doi.org/10.1016/j.ceramint.2022.09.326>

Received 21 July 2022; Received in revised form 9 September 2022; Accepted 25 September 2022

Available online 28 September 2022

0272-8842/© 2022 The Authors. Published by Elsevier Ltd. This is an open access article under the CC BY-NC-ND license (<http://creativecommons.org/licenses/by-nc-nd/4.0/>).

phosphates (CaPs) [14]. CaP ceramics have been extensively studied for their use in bone tissue engineering (BTE) and drug delivery given their similarity to the mineral phase of bone. Among CaPs, synthetic hydroxyapatite (HA,  $\text{Ca}_{10}(\text{PO}_4)_6(\text{OH})_2$ ) has been widely researched as a drug carrier thanks to its great adsorption capacity [15]. However, synthetic HA is extremely stable under physiological conditions with very low *in vivo* biodegradation, which limits its clinical application as a delivery system. As not only HA, but most CaPs are relatively insoluble, it is necessary to investigate more soluble materials that can be used to fabricate hollow spheres.

The incorporation of certain trace elements into synthetic materials like HA can help improve their dissolution rate under physiological conditions [2]. Of them, strontium (Sr) is known to play an important role in the bone regeneration process by stimulating bone formation and inhibiting bone resorption.  $\text{Sr}^{2+}$  ions (1.18 Å) have the same physiological and chemical behavior as  $\text{Ca}^{2+}$  ions (1.00 Å) and can replace Ca in the HA structure up to a full substitution [2]. The incorporation of  $\text{Sr}^{2+}$  ions into HA can increase its solubility by destabilizing the crystal structure of HA [16–18]. Strontium phosphate (SrP) ceramics, such as tribasic strontium phosphate ( $\text{Sr}_3(\text{PO}_4)_2$ ), strontium hydroxyapatite ( $\text{Sr}_5(\text{PO}_4)_3\text{OH}$ ) and strontium hydrogen phosphate ( $\text{SrHPO}_4$ ) with greater biodegradability, can be used as an alternative to more insoluble CaPs for drug delivery [19–21].

Although these carriers have excellent delivery capacity, their mechanical properties do not allow them to be shaped into more complex structures that can support the bone regeneration process. For this reason, three-dimensional (3D) porous scaffolds with better mechanical properties have been used in combination with therapeutic agents to reconstruct bone defects [22]. However, these molecules are normally adsorbed on the scaffold's surface and show a significant burst release once scaffolds have been implanted in the body [23]. Therefore, it is necessary to achieve a more controlled release to improve the therapeutic effect of the administered drugs. By combining both structure types, it is possible to locally release therapeutic agents at the injured site and at the same time, support new bone tissue formation. To date, only a few studies have reported the incorporation of nano-/micro-spheres into 3D scaffolds to achieve sustained drug release. For instance, Son et al. [24] fabricated HA scaffolds containing PLGA microspheres loaded with the anti-inflammatory drug dexamethasone (DEX) and studied their bone regeneration capacity. After 10 weeks of *in vivo* implantation in femur defects of beagle dogs, they observed significant new cortical bone formation in the implanted regions. Conversely, traumatized regions that were either unfilled or filled with DEX-free HA scaffolds presented less bone formation.

In the present work, in order to develop 3D porous scaffolds with controlled delivery capacity, SrP hollow nano-/micro-spheres synthesized by a template-free hydrothermal method were incorporated into ceramic scaffolds. The reaction conditions influencing the synthesis of spheres, such as the hydrothermal temperature, reaction time and concentration of reactants were studied. Moreover, the mechanical properties and *in vitro* bioactive capacity of the scaffolds with incorporated spheres were also investigated.

## 2. Materials and methods

### 2.1. Synthesis and characterization of SrP hollow spheres

Hollow spheres were synthesized by the hydrothermal method without any surfactant or template [13]. First, two solutions were prepared: one containing 0.9 mM of strontium nitrate ( $\text{Sr}(\text{NO}_3)_2$ , Sigma-Aldrich) and 0.9 mM of magnesium chloride ( $\text{MgCl}_2$ , Sigma-Aldrich), and another solution containing 10 mM of disodium hydrogen phosphate ( $\text{Na}_2\text{HPO}_4$ , Sigma-Aldrich), dissolved in 100 mL of deionized water, respectively. Both solutions were mixed under continuous stirring at room temperature and transferred to a teflon-lined stainless-steel autoclave where the hydrothermal reaction was

conducted at 120 °C for 24 h, followed by cooling to room temperature naturally. The resulting precipitates were collected by centrifugation (4500 rpm, 5 min) (Hermle Z 206 A, Germany), washed with ethanol and deionized water several times, and dried at 60 °C for 24 h.

The morphology, microstructure, size distribution and elemental composition of the synthesized products were investigated by scanning electron microscopy with energy dispersive X-ray spectroscopy (SEM-EDX, Hitachi S – 3500 N, Japan). Samples were palladium-coated before observation.

The phase composition of the prepared spheres was characterized by X-ray diffraction (XRD, Bruker, AXR D8 Advance, Germany) using Cu-K $\alpha$  radiation (1.54056 Å). The X-ray tube was operated at 40 kV and 30 mA. Data was collected in the Bragg-Brentano theta-2theta ( $\theta/2\theta$ ) geometry between 20° and 46° ( $2\theta$ ) at 0.02 steps, counting 8 s per step. Diffractograms were analyzed with the Match! 3 software (v. 3.13.0.220) and compared with the Crystallography Open Database (COD) and the International Centre for Diffraction Data (ICDD).

The specific surface area, pore size distribution and pore volume of the spheres were evaluated by the Brunauer-Emmett-Teller (BET) and Barrett-Joyner-Halenda (BJH) methods, applied to the  $\text{N}_2$  adsorption/desorption isotherms. Isotherms were measured with a surface area and porosity analyzer (Autosorb-6, Quantachrome Instruments, USA) at 77 K.

### 2.2. Scaffold synthesis and incorporation of hollow spheres

Multilayer porous scaffolds were prepared by the sol-gel method in combination with the polymeric sponge replication method [25]. First, a sol-gel solution with a composition of  $2\text{SiO}_2$ – $50\text{CaO}$ – $48\text{P}_2\text{O}_5$  (mol%) was prepared for the scaffolds' core. In the initial step, 0.2 mL of tetraethyl orthosilicate (TEOS,  $\text{Si}(\text{OC}_2\text{H}_5)_4$ , Aldrich 98%), 10.5 mL of triethyl phosphate (TEP,  $(\text{C}_2\text{H}_5)_3\text{PO}_4$ , Aldrich  $\geq 99.8\%$ ), 5 mL of ethanol 97°, 20 mL of distilled water and 10 mL of hydrochloric acid (HCl 37%, Ensure) were mixed together under continuous stirring at room temperature for 30 min to allow the hydrolysis of precursors. After this time, 9.5 g of calcium carbonate ( $\text{CaCO}_3$ , Sigma  $\geq 99\%$ ) were added to the solution and the pH was adjusted between 2 and 3 by adding HCl drop by drop. Polyurethane sponges (20 ppi, 12.7 mm diameter, 10 mm high) were immersed in the resulting solution for the appropriate number of times and dried in a furnace (Naberthen, Lilienthal/Bremen, Germany) for 10 min at 180 °C after each immersion. Finally, the coated sponges were sintered at 950 °C at a heating rate of 19 °C/h for 50 h and then maintained at this temperature for 8 h.

Second, another sol-gel solution with composition  $29\text{SiO}_2$ – $66\text{CaO}$ – $3\text{P}_2\text{O}_5$ – $2\text{MgO}$  (mol%) was prepared for the external/bioactive layers of scaffolds. For this purpose, 10.9 mL of TEOS, 1.6 mL of TEP, 5 mL of ethanol 97°, 20 mL of distilled water, 10 mL of HCl, 11 g of calcium carbonate and 0.3 g of magnesium carbonate ( $\text{MgCO}_3$ , Sigma-Aldrich) were mixed following the same procedure described above. The previously obtained scaffolds' core was coated with the new solution and dried at 180 °C for 5 min. After the appropriate number of immersions, multilayer scaffolds were sintered again at 950 °C at a heating rate of 119 °C/h for 8 h and maintained at this temperature for 3 h. The obtained scaffolds were physically, chemically and mineralogically characterized by SEM-EDX and XRD.

Incorporation of spheres was conducted by immersing scaffolds in 50 mL of an ethanol solution containing 0.1 g of the previously synthesized spheres, followed by shaking in a water bath at 37 °C for 4 h. After this time, scaffolds were washed several times with deionized water to remove non-incorporated spheres and dried at 60 °C before analyzing them by SEM-EDX.

Scaffolds' mechanical properties were determined before and after the incorporation of spheres by a simple compression test using a simple manual test stand (SVL-1000 N, IMADA). Tests were carried out by manually applying load to scaffolds (9.1 mm diameter, 7.6 mm high) until their structure collapsed.

Scaffolds' porosity and pore size distribution were examined by the mercury porosimetry technique (Poremaster 60 GT, Quantachrome Instruments, USA) at a pressure between 78.4 bar and 4049.21 bar.

### 2.3. *In vitro* bioactivity of scaffolds with incorporated spheres

The bioactivity of scaffolds with incorporated hollow spheres was tested by immersion in simulated body fluid (SBF) solution prepared according to the procedure established by Kokubo and Takadama [26]. Scaffolds were immersed in 50 mL of SBF (pH 7.4) at 37 °C in a water bath for 3, 7, 14 and 21 days. After each time period, scaffolds were dried at 60 °C for 24 h and their bioactivity was determined by SEM-EDX, assessing apatite formation on scaffolds' surface. Changes in the concentration of Ca, P, Si, Sr and Mg ions released from scaffolds were analyzed by inductively coupled plasma optical emission spectrometry (ICP-OES PerkinElmer Optima 2000™).

## 3. Results

### 3.1. Synthesis and characterization of the CaP scaffolds

The scaffolds obtained by the sol-gel and polymer sponge replication methods were physically and chemically characterized. The microstructure and elemental composition of scaffolds' core were analyzed by SEM-EDX. Scaffolds had an interconnected porosity and were formed by hexagonal grains of Ca, O and P with a Ca/P ratio of ~1.0, which corresponds to the stoichiometric value of calcium pyrophosphate (CPP,  $\text{Ca}_2\text{O}_7\text{P}_2$ ). Scaffolds' XRD pattern confirmed that they were composed of a main CPP phase (COD-96-100-1557). Diffraction peaks were sharp and narrow, which indicate the material's high crystallinity. No other phases were observed in the XRD pattern (Fig. 1b).

Fig. 2 shows scaffolds' pore size distribution, which was determined by the mercury porosimetry technique. Scaffolds had a porosity value of 37.79%, 23.73% of which corresponded to interparticle spaces (<300  $\mu\text{m}$ ), with a pore size between 169.80 and 11.54  $\mu\text{m}$ . The other 14.05% corresponded to intraparticle spaces (<1  $\mu\text{m}$ ), with a pore size between 0.8 and 0.01  $\mu\text{m}$ .

Scaffolds' compressive strength was tested before and after the incorporation of hollow spheres. The scaffolds without spheres had a compressive strength of around 1.27–1.93 MPa, while their mechanical strength after incorporating spheres was 1.56–1.98 MPa. The attachment of spheres had no significant effect on scaffolds' mechanical properties.

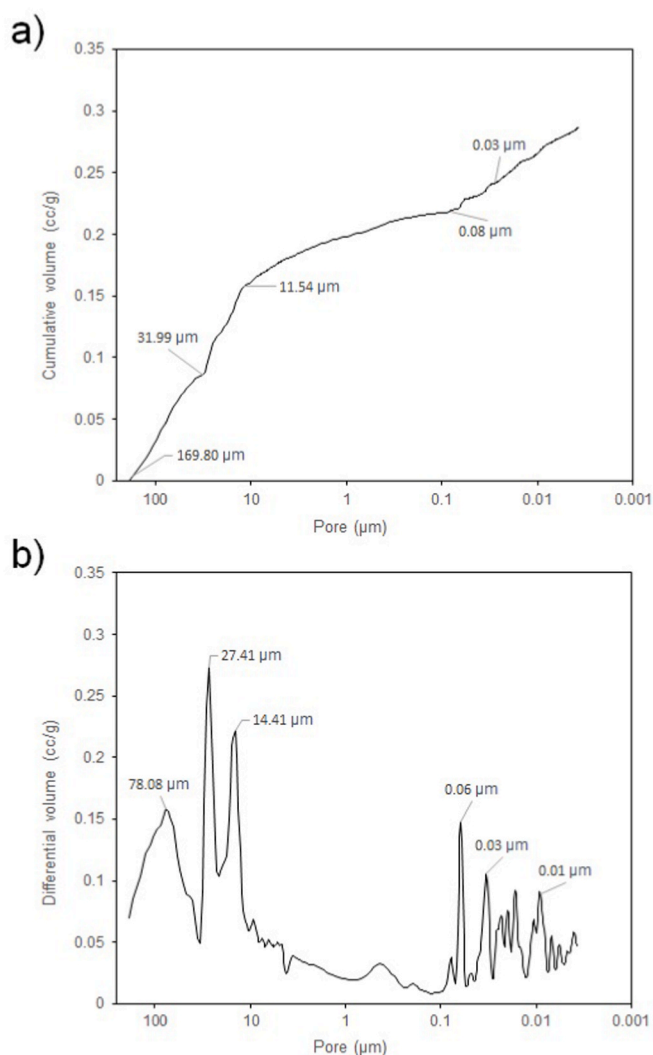


Fig. 2. Mercury porosimetry curves: (a) cumulative and (b) differential intruded volume vs. pore diameter.

### 3.2. Synthesis and characterization of the SrP hollow spheres

The morphology, microstructure, size and elemental composition of the synthesized spheres were studied by SEM-EDX. Fig. 3 shows SEM

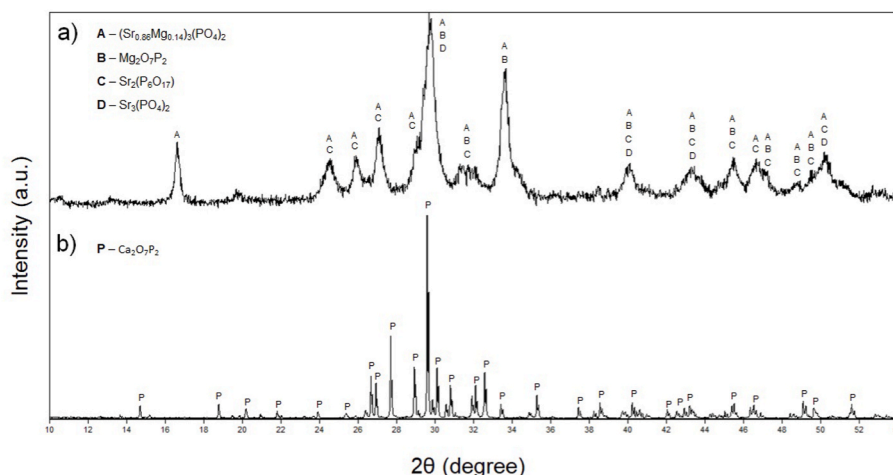


Fig. 1. XRD patterns of the: (a) SrP hollow spheres synthesized at 120 °C for 24 h and (b) 3D CaP porous scaffolds.

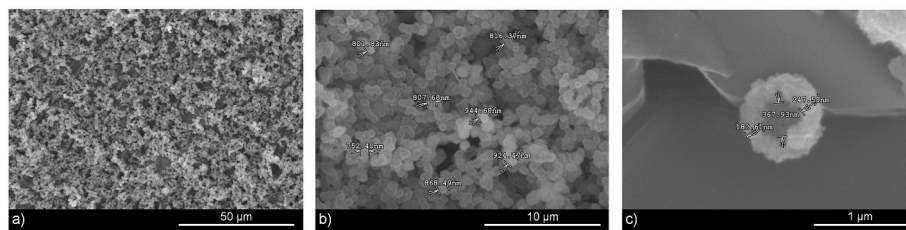


Fig. 3. SEM images of the SrP hollow spheres: (a) low-magnification; (b) size distribution of spheres and (c) broken hollow sphere with details of its dimensions.

images of the spheres prepared by the hydrothermal method at 120 °C for 24 h. A large quantity of spherical precipitates was obtained (Fig. 3a) with an average size of around 850 nm (Fig. 3b). Fig. 3c shows a high-magnification image of a broken sphere, which confirms their hollow structure. EDX analysis was used to determine the elemental composition of precipitates. Hollow spheres were composed of Sr, P, O and Mg, and their Sr/P ratio was about 1.0.

Fig. 1a depicts the phase composition of the hollow spheres determined by XRD. The XRD pattern of these spheres revealed that they were composed of a main Mg-substituted strontium phosphate phase ( $\text{Sr}_{0.86}\text{Mg}_{0.14}\text{P}_3(\text{PO}_4)_2$  (ICDD-00-047-1895), along with some minor phases like magnesium pyrophosphate ( $\text{Mg}_2\text{O}_7\text{P}_2$ ) (COD-96-201-7953), tribasic strontium phosphate ( $\text{Sr}_3(\text{PO}_4)_2$ ) (COD-96-154-4728) and strontium ultraphosphate  $\text{Sr}_2(\text{P}_6\text{O}_{17})$  (COD-96-152-7089).

Fig. 4 shows the  $\text{N}_2$  adsorption/desorption isotherms and the corresponding pore size distribution curve of the hollow spheres. Samples presented a type IV isotherm with an H3 hysteresis loop, which is characteristic of mesoporous materials according to the IUPAC classification [27]. The specific surface area, pore size distribution and pore volume of the shell of spheres were measured by applying the BET and BJH methods to the  $\text{N}_2$  adsorption/desorption isotherms. The BET specific surface area ( $S_{\text{BET}}$ ) of spheres was 30.5  $\text{m}^2/\text{g}$ , while the average pore size and volume were 3.8 nm and 0.14  $\text{cm}^3/\text{g}$ , respectively.

Different synthesis parameters were tested to study the formation process and to determine the best conditions to obtain a large quantity of well-defined hollow spheres. The SEM images of the spherical particles obtained after 6, 12 and 24 h of hydrothermal treatment are shown in Fig. 5. After only 6 h, particles with a spherical morphology were observed (Fig. 5a). After 12 h, precipitates were more defined and slightly larger (Fig. 5b). When prolonging the reaction time to 24 h, the

obtained particles were more spherical and less aggregated (Fig. 5c). Their size also increased and was in the range of 750–950 nm.

The effect of the Mg concentration and reaction temperature on the synthesis of spheres was also investigated. When Mg was absent, no spheres were obtained, and flower-like particles were observed instead (Fig. 6a). With 0.45 mM of Mg, the spherical particles precipitated (Fig. 6b), but in a smaller amount compared to 0.9 mM (Fig. 6c). Mg appears to be essential for the formation of spherical particles.

Regarding the synthesis temperature, different conditions (30, 60 and 120 °C) were tested (Fig. 7). No precipitate was obtained at 30 °C of reaction temperature. At 60 °C, some spherical precipitates formed, but the number of precipitates was small (Fig. 7a). A large quantity of spherical precipitates formed as a result of increasing the reaction temperature to 120 °C (Fig. 7b).

After studying the synthesis process, the obtained precipitates were hydrothermally treated again to observe the effect of a second reaction on the synthesized spheres' morphology. Fig. 8 shows the SEM images of the spheres obtained after 24 h of a second hydrothermal treatment at 120 °C. Afterwards, the precipitates' morphology became more irregular (Fig. 8a), and even more open hollow spheres were observed (Fig. 8b).

### 3.3. Incorporation of the SrP hollow spheres into CaP scaffolds

In order to incorporate the previously synthesized hollow spheres, the CaP porous scaffolds were immersed in an ethanol solution with 0.1 g of dispersed spheres and kept at 37 °C for 4 h. Fig. 9 shows the SEM images of scaffolds' surface with the incorporated spheres. Fig. 9a depicts the scaffolds' surface prior to the incorporation of spheres. After the immersion period, the SrP hollow spheres were homogeneously distributed all over the surface (Fig. 9b). Their morphology and size remained the same after their incorporation (Fig. 9c). Some areas presented larger quantities of aggregated spheres than others, which was probably due to the scaffolds' microstructure (Fig. 9d). The EDX analysis was consistent with those obtained for scaffolds and spheres alone. Hollow spheres were composed of Sr, P, O and Mg, with an Sr/P ratio of 1.0, while the areas without spheres consisted of Ca, O and P, with a Ca/P ratio of 1.0.

### 3.4. *In vitro* bioactivity of the scaffolds with incorporated spheres

After the incorporation of spheres, scaffolds' *in vitro* bioactivity was determined by immersion in SBF for 3, 7, 14 and 21 days. After soaking for 3 days, the hollow spheres were still attached to scaffolds' surface and no changes were observed in their morphology (Fig. 10a). After 7 days, small precipitates with a globular morphology started to cover scaffolds' surface (Fig. 10b). According to the EDX analysis, precipitates were composed of Ca, P and O, with a Ca/P ratio of about 1.5, which comes close to that of stoichiometric HA (Ca/P ratio of 1.67). After 14 days of immersion in SBF, apatite precipitates were partially dissolved, and many hollow spheres were still observed on the surface (Fig. 10c). Finally, after 21 days, apatite precipitated again and formed a dense layer that covered scaffolds' surface (Fig. 10d).

Fig. 11 shows the changes in the  $\text{Sr}^{2+}$ ,  $\text{Mg}^{2+}$ ,  $\text{Ca}^{2+}$ ,  $\text{Si}^{4+}$  and  $\text{PO}_4^{3-}$  ion concentrations of the scaffolds with spheres, analyzed by ICP-OES after

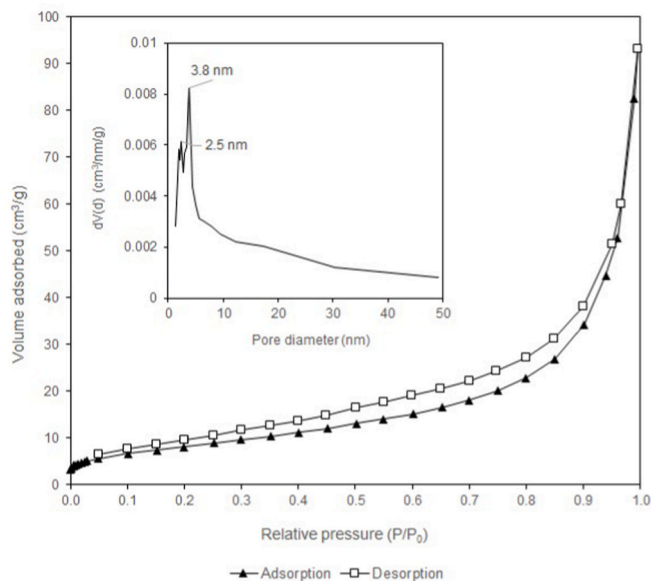


Fig. 4.  $\text{N}_2$  adsorption/desorption isotherms and BJH pore size distribution (inset) of the SrP hollow spheres.

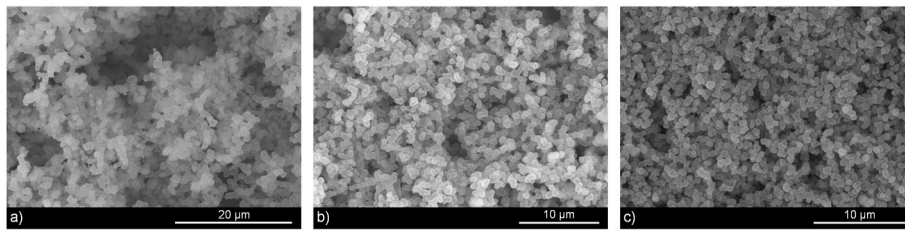


Fig. 5. SEM images of the SrP hollow spheres after different synthesis times at 120 °C: (a) 6 h; (b) 12 h and (c) 24 h.

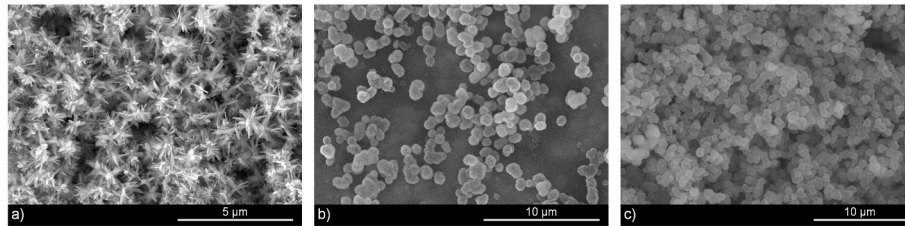


Fig. 6. SEM images of the SrP hollow spheres prepared with different Mg concentrations at 120 °C for 24 h: (a) without Mg; (b) 0.45 mM and (c) 0.9 mM of Mg.

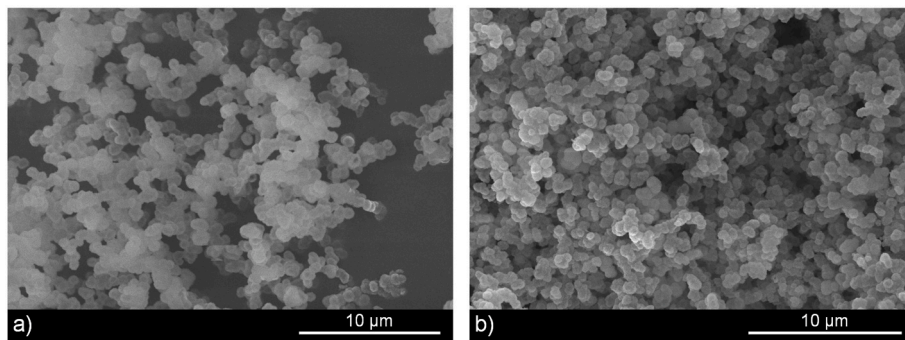


Fig. 7. SEM images of the SrP hollow spheres synthesized at different reaction temperatures for 24 h: (a) 60 °C and (b) 120 °C.

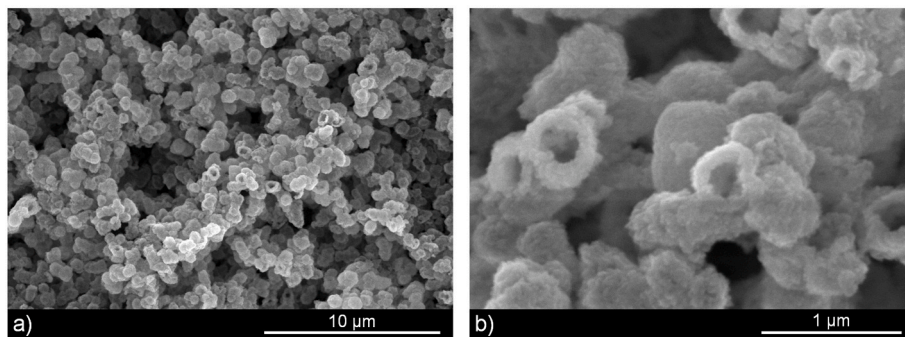


Fig. 8. SEM images of the SrP hollow spheres after a second hydrothermal treatment at 120 °C for 24 h.

the different immersion periods. The  $\text{Ca}^{2+}$  concentration considerably lowered on the first 7 days, after which it slightly rose until day 14, to once again decrease to a final concentration of 47.55 mg/L on the last day. The  $\text{Si}^{4+}$  concentration increased significantly during the experiment, and went from 0.05 mg/L to 14.22 mg/L. On the contrary, the  $\text{PO}_4^{3-}$  concentration dropped throughout the assay and went from an initial value of 28.28 mg/L to a concentration of 11.28 mg/L on day 21.  $\text{Sr}^{2+}$  and  $\text{Mg}^{2+}$  ions were also released to the SBF solution, up to a final concentration of 0.57 mg/L and 31.67 mg/L, respectively.

#### 4. Discussion

The objective of this research was to develop bone substitute materials with increase delivery capacity for bone tissue engineering applications. In this context, the incorporation of a delivery system like hollow spheres directly onto scaffolds, for the local release of therapeutic substances offers the possibility of controlled release at the implant site, improving the bioavailability of substances, while minimizing the possible toxic side effects normally associated with fast burst releases.

Ceramic scaffolds were synthesized by the sol-gel and polymeric

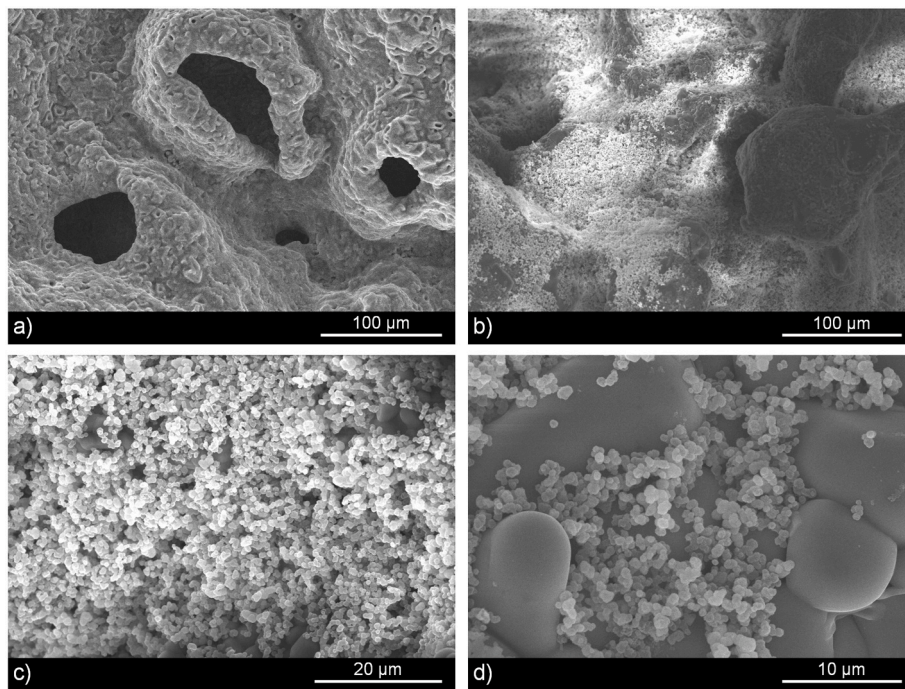


Fig. 9. SEM images of the CaP scaffolds with incorporated SrP hollow spheres: (a) control without spheres; (b) low-magnification and (c, d) high-magnification.

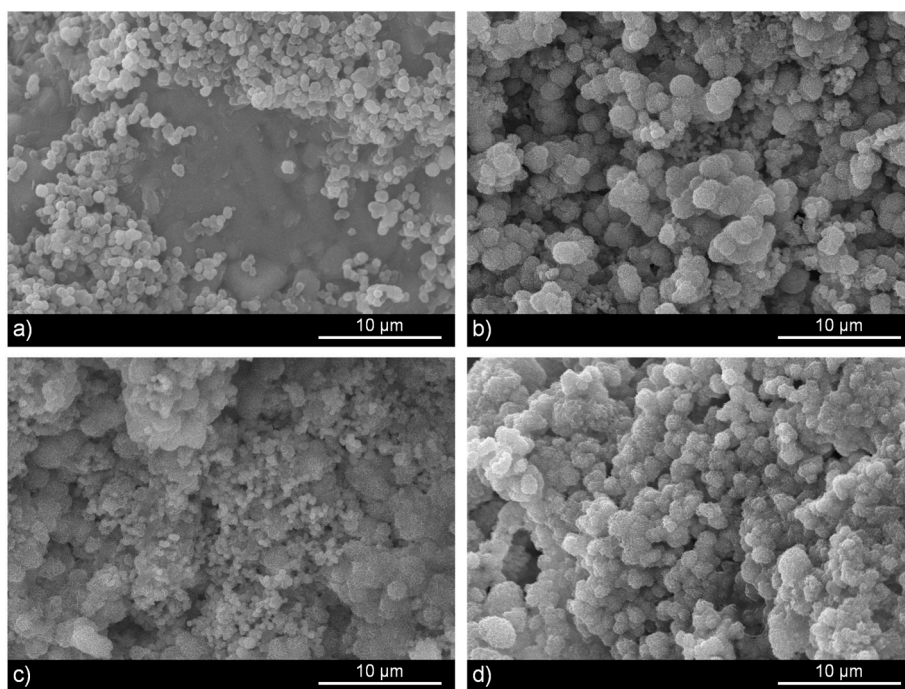


Fig. 10. SEM images of the CaP scaffolds with incorporated spheres soaked in SBF at 37 °C for: (a) 3 days; (b) 7 days; (c) 14 days and (d) 21 days.

sponge replication methods. The combination of these techniques allows us to obtain materials with high interconnected porosity resembling that of trabecular bone in a simple and cost-effective manner and has been commonly employed for the synthesis of 3D porous scaffolds for BTE applications [25,28]. According to SEM observations, scaffolds presented interconnected porosity, which is essential for new bone tissue ingrowth, as it allows the cell migration and proliferation, as well as the vascularization of newly formed tissue [29,30]. Moreover, an interconnected porosity is also necessary for nutrient and metabolic waste transport [22]. Scaffolds' core was composed of Ca, P and O, with a Ca/P

ratio of about 1.0, which corresponds to that of CPP ( $\text{Ca}_2\text{O}_7\text{P}_2$ ), a type of CaP formed by the pyrophosphate anion ( $\text{P}_2\text{O}_7^{4-}$ ). As confirmed by the XRD analysis, scaffolds consisted of a main CPP phase (COD-96-100-1557), which indicates the materials' high purity (Fig. 1b).

Scaffolds had a total porosity value of 37.79% and a pore size distribution within the 169.80–0.01  $\mu\text{m}$  range (Fig. 2). The largest mercury intrusion volume corresponded to interparticle spaces (23.73%), with pores of around 78.08  $\mu\text{m}$ , 27.41  $\mu\text{m}$  and 14.41  $\mu\text{m}$ . The rest of the intruded volume corresponded to intraparticle spaces (14.05%) with an

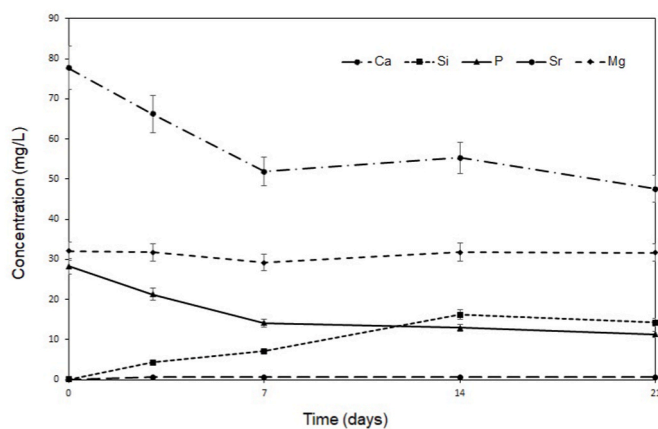


Fig. 11. Changes in the  $\text{Sr}^{2+}$ ,  $\text{Mg}^{2+}$ ,  $\text{Ca}^{2+}$ ,  $\text{Si}^{4+}$  and  $\text{PO}_4^{3-}$  concentrations after immersion in SBF for 3, 7, 14 and 21 days.

average pore size of 0.06  $\mu\text{m}$ . Scaffolds' porosity is one of the key aspects that needs to be considered when designing these structures, because an adequate porosity is necessary for effective bone regeneration. According to pore size, porosity can be classified into two categories: macroporosity ( $>100 \mu\text{m}$ ), which is necessary for cellular colonization as well as vascularization and microporosity ( $<10 \mu\text{m}$ ), which increases ionic exchange and protein adsorption [22,31]. Scaffolds had an adequate pore size, but their total porosity was slightly lower than that of trabecular or cancellous bone, which is in the range of 50–90% [30].

Scaffolds' mechanical properties are important for their possible application in BTE, because they need to be able to withstand sufficient pressure during surgery and new bone tissue formation. Their compressive strength before and after incorporating the hollow spheres was about 1.51 MPa and 1.78 MPa, respectively. The scaffolds with incorporated spheres presented a similar compressive strength to that of the scaffolds alone. In both cases, these values are among the highest for porous ceramic scaffolds, where values of 0.9–1.6 MPa and 1.0–1.7 MPa have been reported [32,33]. Although these values are lower than that of the trabecular bone, ranging between 2 and 12 MPa [34], it is generally accepted that the scaffolds' mechanical strength increases considerably with new bone tissue ingrowth [9].

To control the local release of therapeutic substances from scaffolds, their surface morphology was modified by incorporating hollow spheres as a drug delivery system. Hollow spheres were synthesized by a template-free hydrothermal method, which is a solution-based approach, that allows us to obtain particles with a defined morphology and composition under conditions of high temperature and pressure. This method has been commonly used for the fabrication of hollow spheres over the past few years [8,10].

The morphology of the particles obtained by the hydrothermal method was spherical with hollow interiors of about 350 nm in size, as the observation of some broken or not fully formed spheres revealed (Fig. 3c). They had a rough surface because they were probably formed by many small crystallites, and a shell thickness of about 196 nm. The EDX analysis of spheres revealed that they were composed of Sr, P, O and Mg, with an Sr/P ratio of 1.0, which corresponds to that of strontium hydrogen phosphate ( $\text{SrHPO}_4$ ). The synthesized spheres had a marked tendency to aggregate with one another, which is a common thing in the synthesis of nano-/microparticles ( $<1\text{--}10 \mu\text{m}$ ), which are much more prone to agglomeration than larger particles [12,13]. Moreover, the drying process is a very critical step, particularly in the presence of water, as it can promote the agglomeration of previously loose particles.

The size of spheres was in the range of 600 nm–1  $\mu\text{m}$  and varied slightly with the synthesis conditions. Hollow spheres with sizes of 300–650 nm and 0.8–2  $\mu\text{m}$  have been successfully employed to load drugs like alendronate [35] and doxorubicin [10], respectively.

Therefore, according to the previous literature, the size of the herein synthesized SrP hollow spheres would be appropriate for drug delivery applications.

XRD analysis was conducted to determine the phase composition and crystallinity of the synthesized spheres (Fig. 1a). Precipitates consisted of a main Mg-substituted strontium phosphate phase ( $(\text{Sr}_{0.86}\text{Mg}_{0.14})_3(\text{PO}_4)_2$ ) and some minor phases:  $\text{Mg}_2\text{O}_7\text{P}_2$ ,  $\text{Sr}_3(\text{PO}_4)_2$  and  $\text{Sr}_2(\text{P}_6\text{O}_{17})$ . The broad and weak diffraction peaks indicated that spheres had poor crystallinity, which could be due to them being composed of nanometer-sized crystals, to the ionic substitution of  $\text{Mg}^{2+}$  for  $\text{Sr}^{2+}$  ions in the apatite lattice, or a combination of both [13,36,37]. Whatever the reason, materials with low crystallinity are known to have higher biodegradation rates.

To determine the specific surface area and porous structure of the hollow spheres, the BET and BJH methods were applied to the  $\text{N}_2$  adsorption/desorption isotherms (Fig. 4). Spheres had a mesoporous structure with a pore size distribution between 1.43 and 7.75 nm, and an average pore size of 3.8 nm. Mesopores probably formed due to the existing spaces between nanocrystals in the shell of spheres [38]. Moreover, a pore size of  $\sim 3 \text{ nm}$  is considered appropriate for the effective loading and release of various drugs [39]. A high surface area and a mesoporous structure are important characteristics for an efficient adsorption and release of compounds [29,40]. These characteristics, together with their hollow interiors, confer them a much greater loading capacity compared with other types of structures, which make them ideal candidates to be used as drug carriers.

Regarding the hollow structure formation, we believe that a dissolution-recrystallization process, also known as Ostwald ripening, was the underlying mechanism responsible for the formation of hollow spheres. During the hydrothermal reaction, the inner crystallites gradually dissolve and move outwards, where outer crystallites serve as nucleation points for subsequent recrystallization. With enough ripening time, solid core dissolution results in the formation of hollow spheres [40].

It is known that precipitates' morphology and size very much depend on the hydrothermal temperature, reaction time and concentration of reactants [35,41]. To study the synthesis process, and to determine optimal hydrothermal conditions, different reaction parameters were studied. First, time-dependent experiments were conducted at a fixed temperature of 120  $^\circ\text{C}$ . Fig. 5 shows SEM images of the SrP hollow spheres synthesized for different reaction times. After a 6 h hydrothermal reaction time, some spherical particles had formed, and hollow spheres were observed after 12 h. Prolonging the reaction time to 24 h gave the best results, with well-defined and less aggregated spherical particles. Moreover, with longer synthesis times, more hollow particles are expected to form, as solid to hollow transformation is a time-dependent process [35].

Another key factor in the formation of spherical particles, apart from the reaction temperature and time, is the concentration of reactants, and Mg is particularly known to be a microstructural modifier [13]. To investigate the influence of Mg on precipitates' morphology, different Mg concentrations were used to synthesize hollow spheres. As shown in Fig. 6a, the particles obtained when Mg was absent were not spherically shaped, and instead presented a flower-like morphology. When the Mg concentration was increased to 0.45 mM and especially to 0.9 mM, spherical particles formed. Mg plays a critical role in the formation of spheres because it causes the distortion of the crystal structure, inhibiting crystal growth and allowing for self-assembly into spherical particles [13,42]. It is important to note that changes in the concentrations of Sr and P precursors had no significant effect on precipitates' morphology and size, being Mg the most important element for the formation of spheres.

The hydrothermal reaction temperature is also an important factor that influences precipitates' crystallinity and morphology [41,43]. Therefore, different synthesis temperatures (30, 60 and 120  $^\circ\text{C}$ ) were studied (Fig. 7). The 30  $^\circ\text{C}$  reaction temperature were insufficient and no

precipitate was obtained. At 60 °C, some spherical particles were observed, but the number of precipitates was relatively small. Conversely, with 120 °C, many precipitated spheres formed. High temperatures are essential for the formation of hollow structures because they promote the dissolution and diffusion of the inner crystallites from the solid core to the outer shell.

When spheres were hydrothermally treated a second time, a change in their morphology was observed. Particles presented a less spherical shape and, more importantly, a larger amount of open hollow spheres was obtained (Fig. 8). This could potentially increase the loading efficiency of therapeutic substances by making it easier for larger amounts of these compounds to adsorb on their open hollow interiors. Afterwards, to prevent a burst release, open hollow spheres can be coated with a biodegradable polymer, such as collagen or PLGA, which can help delay the drug release rate [22,29].

The SEM analysis of scaffolds confirmed that the SrP hollow spheres had been successfully incorporated and were well distributed all along the surface (Fig. 9). This was tested several times and with varying amounts of dispersed spheres, resulting in the successful incorporation of the spheres into the scaffolds' surface each time. Spheres' size and morphology remained the same after their incorporation, and some spheres with their exposed hollow interiors were observed. More importantly, the small dimensions of the synthesized spheres did not affect the scaffolds' interconnected porosity. Hollow spheres attachment most likely occurred via non-covalent bonding like electrostatic interactions between the  $\text{Sr}^{2+}$  of spheres and the  $\text{PO}_4^{3-}$  of the CaP material.

To the best of our knowledge, the incorporation of SrP hollow spheres into CaP porous scaffolds has not been previously reported in the literature. To date, hollow nano-/microspheres made of polymeric or ceramic materials have already been used as carriers for the local delivery of therapeutic substances. Xiao et al. [44] fabricated BMP2-loaded hollow HA microspheres and evaluated their bone regeneration capacity when implanted in rat calvarial defects for up to 6 weeks. The amount of new bone in the defects after 6 weeks was 43%, compared to 17% for defects implanted with microspheres without BMP-2. Furthermore, BMP2-loaded microspheres showed greater bone regeneration than 3D HA scaffolds loaded with twice the amount of BMP-2. However, little resorption of the HA microspheres was observed within the implantation period. Although CaPs like HA have a great adsorption capacity, the release of the adsorbed compounds is often dependent on the resorption rate of the material, which for HA, is known to be very low under physiological conditions [2,15]. In this context, SrPs, which are chemically similar to CaPs, are an interesting alternative. SrP materials are known to be biocompatible, biodegradable, osteoconductive and, in some cases, even osteoinductive [21]. Moreover, SrPs have an adsorption capacity comparable to that of CaPs [17].

Previous studies demonstrate that therapeutic substances can be effectively delivered to injured sites via spherical particles incorporated into bone substitute scaffolds to promote osteogenesis *in vivo* [24,45]. This strategy offers the possibility of a controlled release at the implant site, which improves the bioavailability of the substances while minimizing potential toxic side effects that are normally associated with an uncontrolled burst release. Therefore, the development of bone substitute materials with enhanced delivery capacity represents a topic of interest.

The *in vitro* bioactivity of the CaP scaffolds with incorporated hollow spheres was evaluated by immersion in SBF solution, with an ionic composition similar to that of human blood plasma, as established by Kokubo and Takadama [26]. Prior to the incorporation of spheres, scaffolds were coated with a bioactive composition for the external layers doped with 3% of  $\text{Mg}^{2+}$  ions, which are known to promote apatite nucleation and growth [33]. Fig. 10b shows that after 7 days, bone-like apatite precipitates had formed on scaffolds' surface. These precipitates were composed of Ca, P and O, with a Ca/P ratio of  $\sim 1.5$ , which is slightly lower than the stoichiometric one for HA (1.67), indicating the formation of calcium-deficient hydroxyapatite (CDHA) [9,22]. Apatite

precipitates partially dissolved after 14 days in SBF (Fig. 10c) and precipitated again after 21 days to form a dense layer on the surface (Fig. 10d). The formation of an apatite layer on scaffolds' surface after 7 and 14 days, and especially after 21 days, confirmed the *in vitro* bioactive capacity of the scaffolds with incorporated spheres, which is a desirable characteristic for BTE applications. Furthermore, hollow spheres were still attached to scaffolds' surface after 14 days, which denotes their good stability *in vitro* and their potential capacity for a slow and sustained release of therapeutic substances.

On bioactive materials, it is well known that bone-like apatite forms on the surface due to the ionic exchange between the ceramic material and SBF. Therefore, the changes in the concentrations of  $\text{Ca}^{2+}$ ,  $\text{Si}^{4+}$  and  $\text{PO}_4^{3-}$  ions after the different soaking periods in SBF were analyzed by ICP-OES (Fig. 11). The  $\text{Ca}^{2+}$  concentration lowered on the first 7 days, when the first CDHA precipitates started to appear. After this time, the  $\text{Ca}^{2+}$  concentration slightly rose to one of 55.29 mg/L on day 14, probably due to the partial dissolution of the previously formed precipitates, before lowering again to one of 47.55 mg/L on the last day, which was when CDHA precipitated again. The  $\text{Si}^{4+}$  concentration continuously increased from 0.05 mg/L on the first day to 16.19 mg/L on day 14, when it dropped slightly to a final concentration of 14.22 mg/L. This sustained release of  $\text{Si}^{4+}$  ions is related to scaffold degradation. The  $\text{PO}_4^{3-}$  concentration steadily decreased from 28.28 mg/L to 11.28 mg/L by the end of the experiment, as the  $\text{PO}_4^{3-}$  ions from the SBF reacted with the  $\text{Ca}^{2+}$  ion released from scaffolds to form CDHA, which precipitated on scaffolds' surface.

We also studied the release of  $\text{Sr}^{2+}$  and  $\text{Mg}^{2+}$  ions to determine spheres' degradation behavior. The  $\text{Sr}^{2+}$  concentration increased throughout the assay, going from 0.03 mg/L to a final concentration of 0.57 mg/L on day 21. Moreover, the concentration of  $\text{Sr}^{2+}$  ions released from scaffolds fell within the 0.001 mM–0.2 mM range, which has been demonstrated to stimulate osteoblast proliferation [31]. The  $\text{Mg}^{2+}$  concentration remained stable and lowered from 32.03 mg/L to about 31.67 mg/L, probably due to the incorporation of the released ions in the CDHA precipitates partially substituting the  $\text{Ca}^{2+}$  ions. The release of  $\text{Sr}^{2+}$  and  $\text{Mg}^{2+}$  ions indicated that spheres started to degrade after the first 7 days.  $\text{Sr}^{2+}$  and  $\text{Mg}^{2+}$  ions can synergistically enhance cell growth and osteoblastic differentiation, while inhibiting osteoclastic activity at the same time [39,46].

We believe that the incorporation of a local delivery system into bone substitute scaffolds is a promising strategy to achieve a controlled release of therapeutic substances for the *in situ* treatment of infected or damaged bone tissue as an alternative to the systemic administration of these substances. In future studies, it would be of interest to load the synthesized spheres with therapeutic agents (i.e., anti-inflammatory drugs, antibiotics, growth factors, etc.) to determine their loading and releasing efficiencies *in vitro*.

## 5. Conclusion

In this study, novel multifunctional 3D CaP porous scaffolds were developed by incorporating SrP hollow nano-/microspheres for enhanced drug delivery capacity. The calcium pyrophosphate scaffolds presented an interconnected porosity, with a porosity value of 37.79%, and a compressive strength of around 1.56–1.98 MPa.

The SrP hollow spheres with a size between 600 nm–1  $\mu\text{m}$  were obtained by a simple hydrothermal method without any surfactant or template, just by adjusting the reaction temperature, time, and the concentration of reactants. Furthermore, to control the opening of spheres and to, thus, be able to introduce drugs of different sizes, a new procedure was developed to achieve their opening prior to the incorporation into the scaffolds. When spheres were hydrothermally treated a second time, more open hollow particles were obtained.

Spheres were incorporated into scaffolds' surface by immersion in an ethanol solution with dispersed hollow spheres at 37 °C for 4 h. The obtained scaffolds presented a large quantity of spheres homogeneously

distributed along the surface, which were superficially adsorbed through electrostatic interactions. The *in vitro* bioactive capacity of the scaffolds with incorporated spheres was also investigated. Scaffolds were bioactive after 7 days in SBF. Furthermore, hollow spheres remained adhered to their surface after 14 days of immersion. These spheres could potentially be used to load and deliver therapeutic agents to enhance the bone regeneration process. Multifunctional scaffolds with incorporated spheres are a promising alternative to the traditional scaffolds currently used in BTE.

### Funding source

This work is part of the project PID2020-116693RB-C21 funded by MCIN/AEI/10.13039/501100011033 Spain. Grant CIAICO/2021/157 funded by Generalitat Valenciana Spain.

### Declaration of competing interest

The authors declare that they have no known competing financial interests or personal relationships that could have appeared to influence the work reported in this paper.

### References

- [1] Y. Xu, L. An, L. Chen, H. Xu, D. Zeng, G. Wang, Controlled hydrothermal synthesis of strontium-substituted hydroxyapatite nanorods and their application as a drug carrier for proteins, *Adv. Powder Technol.* 29 (2018) 1042–1048, <https://doi.org/10.1016/j.apt.2018.01.008>.
- [2] G. Singh, R.P. Singh, S.S. Jolly, Customized hydroxyapatites for bone-tissue engineering and drug delivery applications: a review, *J. Sol. Gel Sci. Technol.* 94 (2020) 505–530, <https://doi.org/10.1007/s10971-020-05222-1>.
- [3] S.F. Soares, T. Fernandes, A.L. Daniel-Da-Silva, T. Trindade, The controlled synthesis of complex hollow nanostructures and prospective applications, *Proc. Math. Phys. Eng. Sci.* 475 (2019), <https://doi.org/10.1098/rspa.2018.0677>.
- [4] C. Zhang, S. Shan, T. Hu, G. Wang, Y. Zhi, H. Su, L. Jiang, Y. Ni, Recent progress on biomedical applications of functionalized hollow hydroxyapatite microspheres, *Ceram. Int.* 47 (2021) 13552–13571, <https://doi.org/10.1016/j.ceramint.2021.01.214>.
- [5] H. Fu, M.N. Rahaman, D.E. Day, R.F. Brown, Hollow hydroxyapatite microspheres as a device for controlled delivery of proteins, *J. Mater. Sci. Mater. Med.* 22 (2011) 579–591, <https://doi.org/10.1007/s10856-011-4250-6>.
- [6] D. Feng, J. Shi, X. Wang, L. Zhang, S. Cao, Hollow hybrid hydroxyapatite microparticles with sustained and pH-responsive drug delivery properties, *RSC Adv.* 3 (2013) 24975–24982, <https://doi.org/10.1039/c3ra44609c>.
- [7] Y. Jiao, Y.P. Lu, G.Y. Xiao, W.H. Xu, R.F. Zhu, Preparation and characterization of hollow hydroxyapatite microspheres by the centrifugal spray drying method, *Powder Technol.* 217 (2012) 581–584, <https://doi.org/10.1016/j.powtec.2011.11.025>.
- [8] Y.J. Guo, Y.Y. Wang, T. Chen, Y.T. Wei, L.F. Chu, Y.P. Guo, Hollow carbonated hydroxyapatite microspheres with mesoporous structure: hydrothermal fabrication and drug delivery property, *Mater. Sci. Eng. C* 33 (2013) 3166–3172, <https://doi.org/10.1016/j.msec.2013.03.040>.
- [9] S.C. Wu, H.C. Hsu, S.K. Hsu, F.W. Lin, W.F. Ho, Preparation and characterization of porous calcium-phosphate microspheres, *Ceram. Int.* 41 (2015) 7596–7604, <https://doi.org/10.1016/j.ceramint.2015.02.084>.
- [10] W. Lai, C. Chen, X. Ren, I.S. Lee, G. Jiang, X. Kong, Hydrothermal fabrication of porous hollow hydroxyapatite microspheres for a drug delivery system, *Mater. Sci. Eng. C* 62 (2016) 166–172, <https://doi.org/10.1016/j.msec.2016.01.055>.
- [11] B. Liu, X. Hu, Hollow micro- and nanomaterials: synthesis and applications, in: *Advanced Nanomaterials for Pollutant Sensing and Environmental Catalysis*, Elsevier, 2019, pp. 1–38, <https://doi.org/10.1016/B978-0-12-814796-2.00001-0>.
- [12] W. Wen-shou, X. Cheng-Yan, Y. Li, S. Wen-Zhu, Controlled synthesis of calcium tungstate hollow microspheres via ostwald ripening and their photoluminescence property, *J. Phys. Chem. C* 112 (2008) 19390–19398, <https://doi.org/10.1021/jp8074783>.
- [13] C. Berg, H. Engqvist, W. Xia, Ion substitution induced formation of spherical ceramic particles, *Ceram. Int.* 45 (2019) 10385–10393, <https://doi.org/10.1016/j.ceramint.2019.02.097>.
- [14] K.M.Z. Hossain, U. Patel, I. Ahmed, Development of microspheres for biomedical applications: a review, *Prog. Biomater.* 4 (2015) 1–19, <https://doi.org/10.1007/s40204-014-0033-8>.
- [15] H. Fu, M.N. Rahaman, R.F. Brown, D.E. Day, Evaluation of bone regeneration in implants composed of hollow HA microspheres loaded with transforming growth factor  $\beta$ 1 in a rat calvarial defect model, *Acta Biomater.* 9 (2013) 5718–5727, <https://doi.org/10.1016/j.actbio.2012.11.017>.
- [16] J. Christoffersen, M.R. Christoffersen, N. Kolthoff, O. Bärenholdt, Effects of strontium ions on growth and dissolution of hydroxyapatite and on bone mineral detection, *Bone* 20 (1997) 47–54, [https://doi.org/10.1016/S8756-3282\(96\)00316-X](https://doi.org/10.1016/S8756-3282(96)00316-X).
- [17] M. Schumacher, M. Gelinsky, Strontium modified calcium phosphate cements - approaches towards targeted stimulation of bone turnover, *J. Mater. Chem. B* 3 (2015) 4626–4640, <https://doi.org/10.1039/c5tb00654f>.
- [18] K. Lin, P. Liu, L. Wei, Z. Zou, W. Zhang, Y. Qian, Y. Shen, J. Chang, Strontium substituted hydroxyapatite porous microspheres: surfactant-free hydrothermal synthesis, enhanced biological response and sustained drug release, *Chem. Eng. J.* 222 (2013) 49–59, <https://doi.org/10.1016/j.cej.2013.02.037>.
- [19] M.H. Frere, The solubility of some strontium phosphates, *Soil Sci. Soc. Am. J.* 26 (1962) 48–51, <https://doi.org/10.2136/sssaj1962.03615995002600010013x>.
- [20] C. Zhang, Z. Cheng, P. Yang, Z. Xu, C. Peng, G. Li, J. Lin, Architectures of strontium hydroxyapatite microspheres: solvothermal synthesis and luminescence properties, *Langmuir* 25 (2009) 13591–13598, <https://doi.org/10.1021/la9019684>.
- [21] H. Shi, T. Wu, J. Zhang, X. Ye, S. Zeng, X. Liu, T. Yu, J. Ye, C. Zhou, Biocompatible  $\beta$ -SrHPO<sub>4</sub> clusters with dandelion-like structure as an alternative drug carrier, *Mater. Sci. Eng. C* 81 (2017) 8–12, <https://doi.org/10.1016/j.msec.2017.07.034>.
- [22] S. Bose, S. Tarafder, Calcium phosphate ceramic systems in growth factor and drug delivery for bone tissue engineering: a review, *Acta Biomater.* 8 (2012) 1401–1421, <https://doi.org/10.1016/j.actbio.2011.11.017>.
- [23] B. Wan, R. Wang, Y. Sun, J. Cao, H. Wang, J. Guo, D. Chen, Building osteogenic microenvironments with strontium-substituted calcium phosphate ceramics, *Front. Bioeng. Biotechnol.* 8 (2020), <https://doi.org/10.3389/fbioe.2020.591467>.
- [24] J.S. Son, M. Appleford, J.L. Ong, J.C. Wenke, J.M. Kim, S.H. Choi, D.S. Oh, Porous hydroxyapatite scaffold with three-dimensional localized drug delivery system using biodegradable microspheres, *J. Contr. Release* 153 (2011) 133–140, <https://doi.org/10.1016/j.jconrel.2011.03.010>.
- [25] P. Ros-Tàrraga, A. Murciano, P. Mazón, S.A. Gehrke, P.N. de Aza, New 3D stratified Si-Ca-P porous scaffolds obtained by sol-gel and polymer replica method: microstructural, mineralogical and chemical characterization, *Ceram. Int.* 43 (2017) 6548–6553, <https://doi.org/10.1016/j.ceramint.2017.02.081>.
- [26] T. Kokubo, H. Takadama, How useful is SBF in predicting *in vivo* bone bioactivity? *Biomaterials* 27 (2006) 2907–2915, <https://doi.org/10.1016/j.biomaterials.2006.01.017>.
- [27] M. Thommes, K. Kaneko, A.v. Neimark, J.P. Olivier, F. Rodriguez-Reinoso, J. Rouquerol, K.S.W. Sing, Physisorption of gases, with special reference to the evaluation of surface area and pore size distribution (IUPAC Technical Report), *Pure Appl. Chem.* 87 (2015) 1051–1069, <https://doi.org/10.1515/pac-2014-1117>.
- [28] S.N.L. Ramlie, N.S.A.N. Sharifulden, H. Mohamad, S.N.F.M. Noor, Sol-gel derived bioactive glass scaffolds incorporated with polyvinyl-alcohol and pluronic P123 polymers using sponge replication technique, *Mater. Today Proc.* 17 (2019) 966–975, <https://doi.org/10.1016/j.matpr.2019.06.463>.
- [29] D. Loca, J. Locs, A. Dubnika, V. Zalite, L. Berzina-Cimdina, Porous hydroxyapatite for drug delivery, in: *Hydroxyapatite (Hap) for Biomedical Applications*, Elsevier, 2015, pp. 189–209, <https://doi.org/10.1016/b978-1-78242-033-0.00009-2>.
- [30] M. Kucharska, K. Walenko, M. Lewandowska-Szumiel, T. Brynk, J. Jaroszewicz, T. Ciach, Chitosan and composite microsphere-based scaffold for bone tissue engineering: evaluation of tricalcium phosphate content influence on physical and biological properties, *J. Mater. Sci. Mater. Med.* 26 (2015), <https://doi.org/10.1007/s10856-015-5464-9>.
- [31] S. Meiningner, C. Moseke, K. Spatz, E. März, C. Blum, A. Ewald, E. Vorndran, Effect of strontium substitution on the material properties and osteogenic potential of 3D powder printed magnesium phosphate scaffolds, *Mater. Sci. Eng. C* 98 (2019) 1145–1158, <https://doi.org/10.1016/j.msec.2019.01.053>.
- [32] P. Ros-Tàrraga, N.A. Mata, A. Murciano, P. Velasquez, P.N. de Aza, Multilayer ceramic materials: a method to link bioactivity and durability, *Ceram. Int.* 45 (2019) 23611–23618, <https://doi.org/10.1016/j.ceramint.2019.08.072>.
- [33] N.A. Mata, P. Ros-Tàrraga, P. Velasquez, A. Murciano, P.N. de Aza, 3D Multiphase Porous Scaffolds of Calcium Phosphates Doping with Silicon and Magnesium, *Boletín de La Sociedad Española de Cerámica y Vidrio*, 2021, <https://doi.org/10.1016/j.bsecv.2021.03.004>.
- [34] T.M. de Witte, L.E. Fratila-Apachitei, A.A. Zadpoor, N.A. Peppas, Bone tissue engineering via growth factor delivery: from scaffolds to complex matrices, *Regen. Biomater.* 5 (2018) 197–211, <https://doi.org/10.1093/rb/rby013>.
- [35] H. Duan, J. Diao, N. Zhao, Y. Ma, Synthesis of hollow mesoporous bioactive glass microspheres with tunable shell thickness by hydrothermal-assisted self-transformation method, *Mater. Lett.* 167 (2016) 201–204, <https://doi.org/10.1016/j.matlet.2015.12.162>.
- [36] H. Zhou, M. Nedley, S.B. Bhaduri, The impacts of Mg<sup>2+</sup> on strontium phosphate: a preliminary study, *Mater. Lett.* 113 (2013) 63–66, <https://doi.org/10.1016/j.matlet.2013.09.079>.
- [37] L. Xiong, J. Zeng, A. Yao, Q. Tu, J. Li, L. Yan, Z. Tang, BMP2-loaded hollow hydroxyapatite microspheres exhibit enhanced osteoinduction and osteogenicity in large bone defects, *Int. J. Nanomed.* 10 (2015) 517–526, <https://doi.org/10.2147/IJN.S74677>.
- [38] H. Duan, Y. Ma, X. Liu, L. Hao, N. Zhao, Hierarchically nanostructured hydroxyapatite microspheres as drug delivery carriers and their effects on cell viability, *RSC Adv.* 5 (2015) 83522–83529, <https://doi.org/10.1039/c5ra11956a>.
- [39] G.K. Pouroutzidou, L. Liverani, A. Theocharidou, I. Tsamesidis, M. Lazaridou, E. Christodoulou, A. Beketova, C. Pappa, K.S. Triantafyllidis, A.D. Anastasiou, L. Papadopoulou, D.N. Bikiaris, A.R. Boccaccini, E. Kontonasi, Synthesis and characterization of mesoporous Mg- and Sr-doped nanoparticles for moxifloxacin drug delivery in promising tissue engineering applications, *Int. J. Mol. Sci.* 2021 (2021) 577, <https://doi.org/10.3390/ijms>.
- [40] S.D. Jiang, Q.Z. Yao, G.T. Zhou, S.Q. Fu, Fabrication of hydroxyapatite hierarchical hollow microspheres and potential application in water treatment, *J. Phys. Chem. C* 116 (2012) 4484–4492, <https://doi.org/10.1021/jp211648x>.

- [41] Y. Zhu, L. Xu, C. Liu, C. Zhang, N. Wu, Nucleation and growth of hydroxyapatite nanocrystals by hydrothermal method, *AIP Adv.* 8 (2018), <https://doi.org/10.1063/1.5034441>.
- [42] T. Qin, P. Zhang, I.H. Wani, Y. Han, K. Leifer, F. Nikolajeff, H. Engqvist, A general strategy for template-free and low-cost synthesis of inorganic hollow spheres, *Powder Technol.* 319 (2017) 163–171, <https://doi.org/10.1016/j.powtec.2017.06.051>.
- [43] M. Sadat-Shojai, M.T. Khorasani, E. Dinpanah-Khoshdargi, A. Jamshidi, Synthesis methods for nanosized hydroxyapatite with diverse structures, *Acta Biomater.* 9 (2013) 7591–7621, <https://doi.org/10.1016/j.actbio.2013.04.012>.
- [44] W. Xiao, H. Fu, M.N. Rahaman, Y. Liu, B.S. Bal, Hollow hydroxyapatite microspheres: a novel bioactive and osteoconductive carrier for controlled release of bone morphogenetic protein-2 in bone regeneration, *Acta Biomater.* 9 (2013) 8374–8383, <https://doi.org/10.1016/j.actbio.2013.05.029>.
- [45] A.H. Yao, X.D. Li, L. Xiong, J.H. Zeng, J. Xu, D.P. Wang, Hollow hydroxyapatite microspheres/chitosan composite as a sustained delivery vehicle for rhBMP-2 in the treatment of bone defects, *J. Mater. Sci. Mater. Med.* 26 (2015) 1–12, <https://doi.org/10.1007/s10856-014-5336-8>.
- [46] F. He, T. Lu, X. Fang, C. Qiu, Y. Tian, Y. Li, F. Zuo, J. Ye, Study on Mg<sub>x</sub>Sr<sub>3-x</sub>(PO<sub>4</sub>)<sub>2</sub> bioceramics as potential bone grafts, *Colloids Surf. B Biointerfaces* 175 (2019) 158–165, <https://doi.org/10.1016/J.COLSURFB.2018.11.085>.